Icarus **157**, 128–138 (2002)
doi:10.1006/icar.2002.6833, available online at http://www.idealibrary.com on IDEAL®

Spatial and Compositional Constraints on Non-ice Components and H_2O on Pluto's Surface

W. M. Grundy and M. W. Buie

Lowell Observatory, 1400 W. Mars Hill Road, Flagstaff, Arizona 86001
E-mail: grundy@lowell.edu

Received September 5, 2001; revised January 3, 2002

We present four new near-infrared spectra of Pluto, measured separately from its satellite Charon during four HST/NICMOS observations in 1998, timed to sample four evenly spaced longitudes on Pluto. Being free of contamination by telluric absorptions or by Charon light, the new data are particularly valuable for studies of Pluto's continuum absorption. Previous studies of the major volatile species indicate the existence of at least three distinct terrains on Pluto's surface: N_2-rich, CH_4-rich, and volatile-depleted. The new data provide evidence that each of these three terrains has distinct near-infrared continuum absorption features. CH_4-rich regions appear to show reddish continuum absorption through the near-infrared spectral range. N_2-rich regions have very little continuum absorption. Visually dark, volatile-depleted regions exhibit intermediate continuum albedos with a bluish continuum slope. By analogy with Triton, we expected that careful spectral modeling would reveal strong evidence for the existence of H_2O ice on Pluto's surface, but we found only very weak evidence for its existence in the volatile-depleted regions. These data require H_2O ice to play a much less prominent role on Pluto's surface than it does on Triton's. © 2002 Elsevier Science (USA)

Key Words: **Pluto surface; ices; spectroscopy; infrared observations.**

1. INTRODUCTION

Vibrational absorption bands of CH_4 ice dominate the near-infrared reflectance spectrum of Pluto, with additional absorptions by N_2 and CO ices compounding the spectrum's complexity. The shapes, wavelengths, and depths of Pluto's ice absorption bands can be used to derive information about the textures, temperatures, and distributions of different ice species on Pluto's surface. However, interpreting the spectral evidence can be quite difficult, as it is hindered by shortages of laboratory data for Pluto's surface materials at appropriate temperatures and thermodynamic conditions as well as by uniqueness problems arising from diverse configurations producing similar spectral effects. Nevertheless, considerable progress in interpreting the spectroscopic data has been made over the past decade (e.g., Owen *et al.* 1993, Tryka *et al.* 1994, Grundy 1995, Quirico 1995), culminating in analyses by Douté *et al.* (1999) of a single very high quality spectrum of one face of Pluto/Charon and by Grundy and Buie (2001) of 83 lower quality spectra of Pluto/Charon, obtained over a three-year interval.

A critical challenge in observing Pluto spectroscopically is that its spectrum is not static. It changes through time in at least three important ways, over various time scales. First, as Pluto spins with a 6.387-day period, geographical regions at different longitudes rotate into view, their albedo variations producing Pluto's pronounced lightcurve. Second, as Pluto follows its heliocentric orbit, different latitudes come into view. The northern polar cap of Pluto is currently coming into view for the first time since before Pluto's discovery, while less and less of the southern hemisphere is visible from Earth each year. Finally, the surface of Pluto itself evolves on seasonal timescales, driven by solar energy. At latitudes receiving the most insolation (the same latitudes Earth-based observations are most sensitive to), nitrogen ice sublimates at rates as high as several centimeters per Earth year, recondensing in regions currently receiving less sunlight. Over time, this sublimation leads to bulk migration of volatile ices (Spencer *et al.* 1997). Seasonal volatile transport is expected to produce significant changes in surface texture (Grundy and Stansberry 2000), may regionally reveal the substrate which underlies the nitrogen ice, and could drive gradual increases in local CH_4 concentration (e.g., Benchkoura 1996, Stansberry *et al.* 1996, Trafton *et al.* 1997, 1998, Stansberry and Yelle 1999), in regions where more volatile nitrogen is preferentially removed.

Long term spectroscopic monitoring over all time scales is the only way to detect and to disentangle these effects. The task is complicated by the presence of Pluto's satellite Charon, which contributes about a fifth of the total surface area of the Pluto/Charon system and has its own distinctive spectral signature (see Fig. 1), as well as phase behavior quite different from that of Pluto (Buie *et al.* 1997a, Buie and Grundy 2000a). The maximum separation between Pluto and Charon is less than an arcsecond as seen from Earth, so the two bodies are difficult to study separately (e.g., Brown and Calvin 2000, Dumas *et al.* 2001), particularly with the types of equipment available for frequent monitoring over many years.

0019-1035/02 $35.00

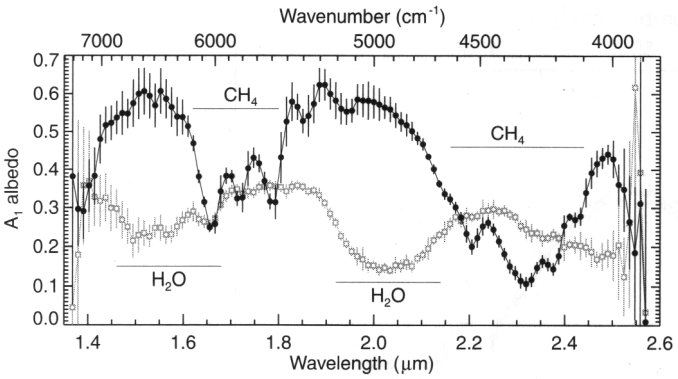

FIG. 1. Grand average of the NICMOS spectra of Pluto (black, filled circles) and Charon (grey, open squares, from Buie and Grundy 2000a) showing their distinct spectral characteristics on a common albedo scale (A_1 albedo is defined in the text). Error bars are based on variations between the spectra obtained at different longitudes; for Pluto, they are dominated by real longitudinal variability. Wavelengths showing strong absorptions by CH_4 and H_2O ices are indicated with horizontal bars.

2. OBSERVATIONS

We undertook HST/NICMOS observations to constrain a model for removing Charon's spectral contribution from blended ground-based observations, as discussed in two companion papers (Buie and Grundy 2000a, Grundy and Buie 2001). The four absolutely calibrated spectra of Pluto alone which we present in this paper were by-products of that effort.

Our observations were scheduled to sample four well-spaced sub-Earth longitudes, as summarized in Table I. Each observation consisted of 11 spatially dithered science exposures taken during a single HST orbit through the G206 grism. The table shows the mid-time of each observation along with the solar phase angle and sub-Earth longitude on Pluto. Extraction of spectra from HST/NICMOS grism images was a complex signal processing task, involving procedures described in detail by Buie and Grundy (2000a). The resulting spectra are shown in Figs. 1 and 2. These spectra have been converted to A_1 albedo, which is analogous to geometric albedo in that it is the ratio of the observed flux to the flux that would be received from a Lambert disk of the same radius, viewed and illuminated normally from the same distances, except that in A_1 albedo, the body is viewed at a phase angle of one degree instead of zero. We use A_1 albedo instead of geometric albedo because Pluto has yet to be observed near zero phase. Not knowing what sort of opposition behavior Pluto exhibits, we do not wish to extrapolate the Buie *et al.* (1997a) phase behavior beyond the range of phase angles for which it was measured.

TABLE I
Summary of Observations

UT Date of observation	Phase angle	Sub-Earth longitude
1998/03/17.8	1.80°	50°
1998/03/27.5	1.68°	223°
1998/05/28.8	0.42°	311°
1998/06/07.3	0.53°	128°

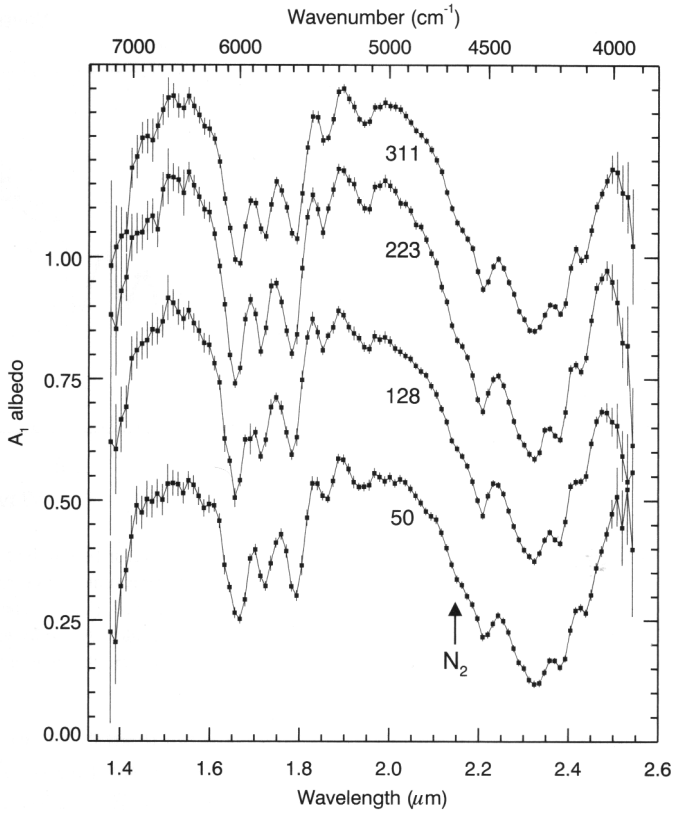

FIG. 2. The four new spectra of Pluto numbered by longitude, as in Table I. The spectra were converted to A_1 albedo using the Buie *et al.* (1997a) phase coefficient for visible wavelengths, as described in the text. All features readily apparent in these spectra are due to vibrational absorptions by CH_4 ice except for the subtle 2–0 β N_2 ice band, indicated by the arrow. The ordinate axes are labeled for the 50° spectrum; other spectra are shifted upward in successive increments of 0.25.

We compare the new NICMOS spectra with recent, higher spectral resolution ground-based spectra of Pluto in Fig. 3. The agreement is quite good, except for a subtle wavelength shift affecting the long-wavelength end of the NICMOS spectra. We found that the addition of a small quadratic term (7×10^{-7} μm pixel^{-2}) to the NICMOS linear dispersion relation could eliminate the discrepancy, and we have applied this term to all data shown in this paper, with the exception of Fig. 3. Note that a discrepancy of this magnitude could not have been detected from the Charon data (Buie and Grundy 2000a), because the H_2O ice features which dominate Charon's spectrum are much broader than the CH_4 ice features which dominate Pluto's spectrum. This type of correction term may be needed for accurate wavelength calibration of all NICMOS/G206 spectra, but we do not have high confidence in its precise magnitude or functional form since the Pluto data are not optimally suited for determining these parameters.

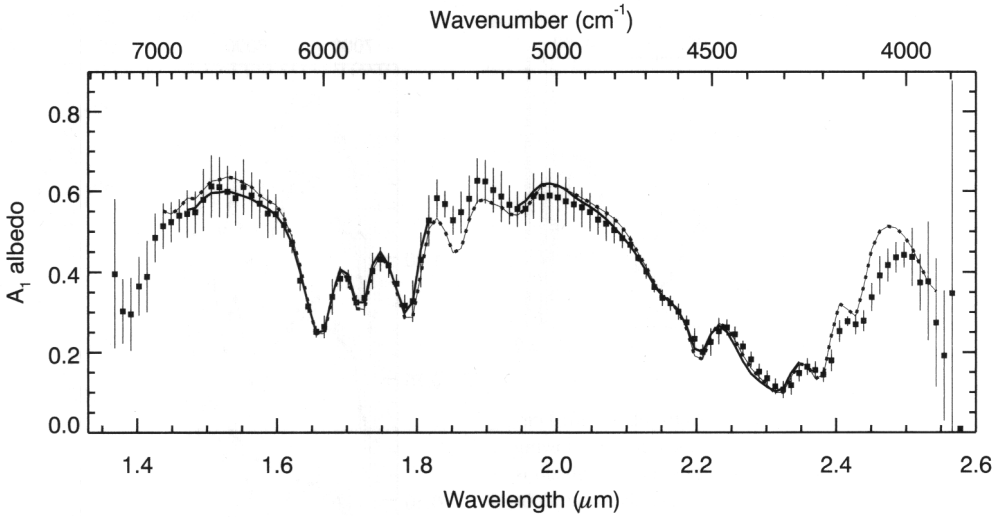

FIG. 3. Grand average of the NICMOS spectra (points; error bars reflect longitudinal spectral variation of Pluto), compared with two ground-based spectra resampled at NICMOS spectral resolution. The thick curve represents the grand average of 83 Pluto spectra published by Grundy and Buie (2001) and the beads-on-a-string curve represents a spectrum published by Douté *et al.* (1999). The Douté *et al.* spectrum differs from the others in having been obtained at a single longitude (200°), while the others are averages over all longitudes. A subtle wavelength calibration discrepancy can be seen at longer wavelengths, with spectral features in the NICMOS data appearing at slightly longer wavelengths than in the other two spectra.

The new HST/NICMOS Pluto data have three distinct advantages over the state of the art in ground-based observations of Pluto/Charon (e.g., Douté *et al.* 1999; Grundy and Buie 2001), even though ground-based observations have higher spectral resolutions and higher signal-to-noise ratios. First, there is no need to depend on an uncertain model to remove the spectral contribution of Charon, since Pluto and Charon were spatially resolved in the HST observations. Second, having been obtained from above the Earth's atmosphere, the NICMOS data are completely uncontaminated by residual telluric absorptions, which are nearly impossible to perfectly cancel from ground-based observations, particularly around ~1.9 μm, where atmospheric water vapor absorbs strongly and variably. Third, the full spectral range from 1.4 to 2.55 μm was recorded simultaneously in a single diffraction order, eliminating uncertainties introduced by patching together separate spectral orders or atmospheric windows.

These three advantages are most valuable for analysis of Pluto's spectral continuum (wavelengths away from strong CH_4, CO, and N_2 absorption bands). Broadband and continuum absorbers such as H_2O ice, salts, silicate minerals, and *tholins* are difficult to study in ground-based spectra in which the splicing together of different wavelength segments and residual telluric absorptions produce uncertainties in spectral slopes and absolute calibration levels. These difficulties typically occur at inconvenient wavelengths for studies of H_2O, since many spectrometers are designed such that their spectral orders coincide with windows between telluric H_2O vapor absorptions. Because continuum absorbers generally have broad absorption features, their study is not particularly impeded by the lower spectral resolution offered by NICMOS, relative to ground-based instruments. Therefore, in the remainder of this paper our attention is primarily directed toward continuum wavelengths and absorbers.

3. ANALYSIS

In this section we examine the HST/NICMOS data set, to see what it can tell us about the compositions and distributions of continuum absorbers on Pluto's surface. We first explore how Pluto's near-infrared lightcurve varies with wavelength. We then consider variations in Pluto's spectral features, taking advantage of the combined spectral and spatial/temporal information contained in the new data to constrain models of Pluto's surface.

3.1. Pluto's Infrared Lightcurve

We begin our analysis of the NICMOS data set by examining Pluto's lightcurve as a function of infrared wavelength. Since the lightcurve is caused by longitudinal albedo variations on Pluto, this approach provides a way of learning about spectral differences between various provinces on Pluto's surface. As shown in Fig. 4, Pluto's lightcurve varies with wavelength through the near-infrared, and can differ considerably from the more familiar V lightcurve (e.g., Buie *et al.* 1997a, Buie and Grundy 2000b).

In the cores of strong CH_4 absorption bands (e.g., at 2.2 and 2.32 μm) Pluto presents a lightcurve which is inverted from its visible lightcurve, implying less CH_4 absorption by terrains which are dark at visible wavelengths and more CH_4 absorption in visually brighter regions. The observed pattern is consistent with the strong CH_4 bands being predominantly formed in the bright, icy regions responsible for producing the visible lightcurve maximum, confirming results published earlier (e.g., Buie and Fink 1987, Marcialis and Lebofsky 1991). However, one cannot conclude from band center albedos or even band depths that CH_4 ice must be less abundant in dark regions, since many factors in addition to abundance influence observed depths of absorption bands (e.g., Grundy and Buie 2001).

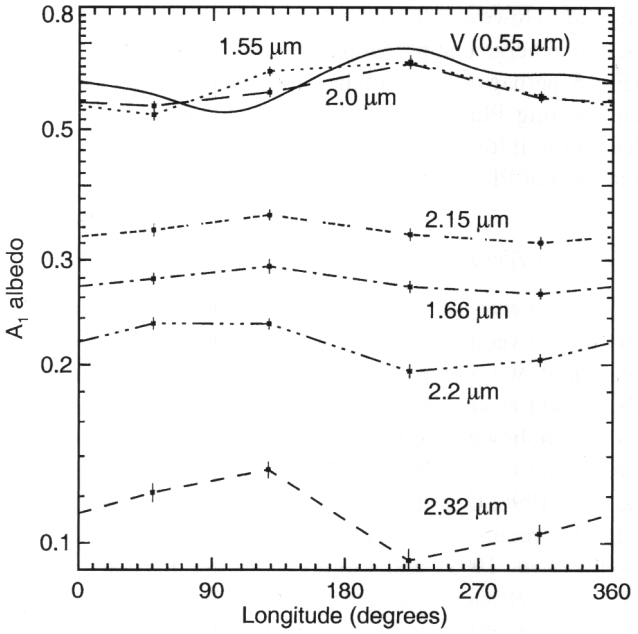

FIG. 4. Pluto lightcurves at several infrared wavelengths (points connected by broken lines), compared with Pluto's visible lightcurve (solid curve from Buie Grundy 2000b).

At continuum infrared wavelengths, where CH_4 absorption is minimal, Pluto's lightcurve looks rather different from what is seen at wavelengths having strong CH_4 absorption. Figure 4 shows the 1.55- and 2.0-μm continuum lightcurves to be quite similar to the visible lightcurve, except for the point at longitude 128° where Pluto is brighter relative to other longitudes than it is at visible wavelengths. It would be reasonable to expect Pluto's lightcurve at near-infrared continuum wavelengths to be similar to its visible lightcurve, since N_2 and CH_4 ices are bright at both visible and infrared continuum wavelengths. If the visible lightcurve were predominantly caused by varying abundance of these bright ices with longitude, that distribution of ices should produce similar lightcurve patterns at infrared continuum wavelengths. So what causes Pluto's infrared continuum albedos to be so high near the minimum of the visible lightcurve? Grundy and Fink (1996) showed that in the 0.5- to 1-μm wavelength range, the reddish slope of Pluto's continuum is greatest near lightcurve minimum. Evidently a visually dark, reddish unit is prominent at those longitudes. The NICMOS data now reveal that this visually dark, reddish material must be much brighter at 1.55 and 2.0 μm.

Pluto's lightcurve at the wavelength of the 2.15 μm N_2 ice absorption band is relatively flat, unlike the larger-amplitude lightcurve behavior seen in the strong CH_4 ice absorption bands and the continuum regions. Apparently, the longitudinal distribution of N_2 ice (e.g., Grundy and Fink 1996, Grundy and Buie 2001) on Pluto's surface is insufficiently heterogeneous to produce a large lightcurve amplitude at 2.15 μm, though the muted lightcurve at 2.15 μm is perhaps not surprising considering the intrinsic weakness of the N_2 ice absorption band. The distribution of N_2 ice may well be irrelevant to Pluto's 2.15-μm lightcurve, if the lightcurve at that wavelength is more strongly influenced by the adjacent, strong 2.2-μm CH_4 ice band than by the weak N_2 ice band. The muted 2.15-μm lightcurve looks quite similar to the 1.66-μm lightcurve, where a weaker CH_4 band is centered.

3.2. Spectroscopic Variations

We next examine Pluto's spectral features to see how they vary with longitude. Significant spectral variations are readily apparent in the HST/NICMOS data, particularly if the spectra are divided by the average over all longitudes from Fig. 1, as shown in Fig. 5.

Rotationally resolved spectroscopy of Pluto has previously been used to characterize the longitudinal distribution of Pluto's surface ice species (e.g., Buie and Fink 1987, Marcialis and Lebofsky 1991, Grundy and Fink 1996). More recently, Grundy and Buie (2001) showed that absorption band strengths for each of the known volatile ice species on Pluto, N_2, CO, and CH_4, exhibit distinctive patterns of variation with Pluto's rotation,

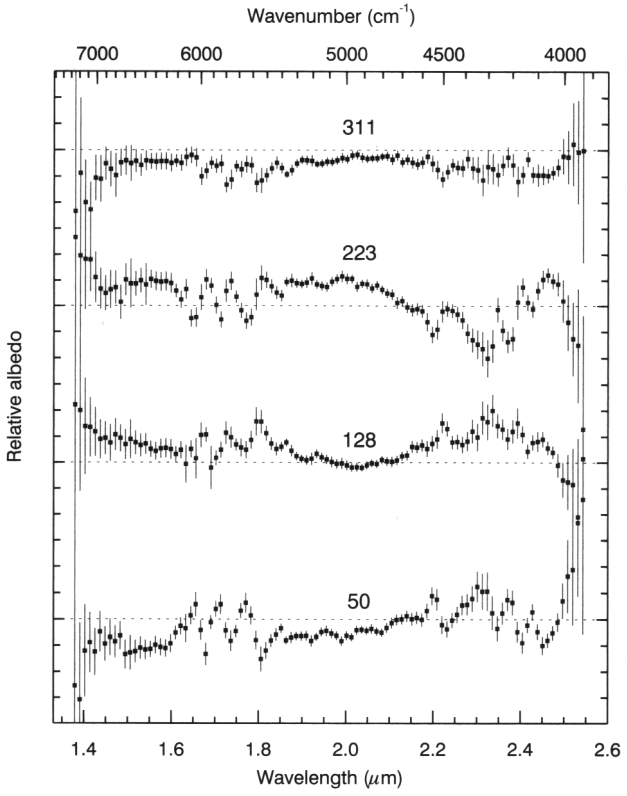

FIG. 5. Ratios of the four Pluto spectra to the grand average from Fig. 1, again numbered by longitude. Longitudinal variations in overall albedo, in continuum slope, and in CH_4 absorption bands are clearly apparent in these ratios. Horizontal dotted lines indicate unity for each ratio. Minor ticks on the ordinate axes mark 10% intervals.

implying a different longitudinal distribution for each ice species. The lower spectral and longitudinal resolution of the NICMOS data makes them less suitable for exploring distributions of ice species; the N_2 band at 2.15 μm can only barely be seen, and we cannot even detect the narrow CO absorption bands at 1.58 and 2.35 μm. However, as discussed earlier, the HST/NICMOS data are most optimal for study of continuum absorbers, so we direct our attention primarily to these components of Pluto's surface.

Many species have previously been considered as potential continuum absorbers on Pluto, such as amorphous carbon, H_2O ice, and organic *tholins*. Other plausible candidates include silicate minerals derived from meteoritic sources, organic ices produced by photolysis and radiolysis of CH_4 in Pluto's atmosphere, and various salts and sulfur compounds brought to Pluto's surface by large impacts and/or cryovolcanic processes (e.g., Delitsky and Thompson 1987, Stern *et al.* 1988, Bohn *et al.* 1994, Grundy and Fink 1996, Cruikshank *et al.* 1997, Grundy and Buie 2001).

Even CH_4 ice contributes to absorption in Pluto's continuum regions, since weak CH_4 ice absorptions are considerably enhanced relative to their stronger counterparts in Pluto's spectrum (Grundy 1995) and CH_4 absorption coefficients are nonzero, even in continuum regions (Schmitt *et al.* 1998, Grundy *et al.* 2001). Unfortunately, accurate optical constants for CH_4 ice are difficult to obtain at these wavelengths because of the difficulty of measuring such weak absorptions in the laboratory (less than 0.1 cm^{-1} for pure CH_4 ice; proportionately less for CH_4 diluted in N_2 ice).

As done in earlier work, ratios between strategically selected wavelengths can be used to obtain a qualitative picture of where specific absorbers are located on Pluto's surface. For example, a ratio between 1.78 and 1.83 μm is sensitive to absorption by CH_4 ice (see Fig. 1). Examining Fig. 5 we note a comparison of ratios between these wavelengths at different longitudes indicates maximum CH_4 absorption in the 223° spectrum, consistent with earlier results (e.g., Marcialis and Lebofsky 1991, Grundy and Buie 2001).

This ratio technique can also be used to study absorption at continuum wavelengths (spectral regions away from strong CH_4 absorption bands). For example, ratios between albedos at 1.5- and 2.0-μm wavelengths are useful for monitoring continuum slopes. Figure 5 shows that the reddest continuum slope in the near-infrared is seen at 50° longitude, while at 128° longitude, the slope is distinctly more blue than the global average. This contrast between 50° and 128° is somewhat surprising, since at CCD wavelengths, the hemisphere centered on ~90° longitude is Pluto's reddest (Grundy and Fink 1996). Perhaps an additional species, concentrated near 128° longitude, absorbs preferentially at 2 μm but not at visible wavelengths. Water ice has a strong 2-μm absorption band (see Fig. 1), is bright in the visible, and is a plausible constituent of Pluto's surface (e.g., Grundy 1995, Cruikshank *et al.* 1997). Buie *et al.* (1999) pointed out that the ratio of 2.00 to 1.89 μm might prove useful for prospecting for water ice on Pluto, and computing this ratio from Fig. 5 does indeed suggest maximum H_2O ice absorption around 128° longitude. However, the distinctive spectral signature of H_2O ice does not emerge unambiguously from the spectral ratios shown in Fig. 5, perhaps because of the numerous other spectral features complicating Pluto's near-infrared reflectance. In an effort to glean more information from our spectral data, we next turned to models of Pluto's surface.

3.2.1. Two-Terrain Model

We begin with a simple model for the continuum spectral differences between Pluto's regions, assuming that Pluto's surface consists of two provinces, one dark at visible wavelengths, the other bright at visible wavelengths. Two-terrain maps have already been shown to be unable to replicate the longitudinal variations of Pluto's CH_4, N_2, and CO absorption bands (e.g., Grundy and Fink 1996, Grundy and Buie 2001). At least three terrains were also required to match the shapes of Pluto's CH_4 bands (Douté *et al.* 1999) and Pluto's thermal emission lightcurve behavior (Lellouch *et al.* 2000). However, two-terrain models remain to be tested in studies of the longitudinal behavior of Pluto's near-infrared continuum wavelengths.

Pluto's visible albedo features have been mapped at low spatial resolution by means of HST/WFPC2 images (Stern *et al.* 1997). By combining albedo map information with the NICMOS data, it is possible to solve for the separate spectra of two terrains by performing the following linear least squares fit at each wavelength. Starting with one of the Stern *et al.* (1997) maps, we converted it to normal albedo. The darkest and brightest regions of the map were assumed to have the spectra of pure end members, while intermediate points were assumed to be albedo-weighted combinations of the two end member spectra. The fractional coverage map thus produced was then projected to the observing geometry of each NICMOS observation. At each wavelength, we solved for the two albedo values to best match the disk-integrated values observed by NICMOS at all four longitudes. The derived end member and disk-integrated spectra are shown in Fig. 6; the reduced χ^2 of the fit was 7 (for only the continuum wavelengths and also for the full data set).

Although at continuum wavelengths, the derived dark end member shows a reddish slope consistent with the reddish character of visually darker regions of Pluto's surface indicated by the infrared lightcurves in Section 3.1, Pluto's continuum albedos are not well matched by the two-terrain model, as shown by an examination of the bottom panel of Fig. 6 (as well as the reduced χ^2 of 7, no better than that obtained for all wavelengths). Model continuum albedos tend to be too high at 311° longitude. The model is also too dark around 1.5 μm at 128° longitude. We conclude that two-terrain models constrained by visible wavelength albedo maps do a poor job of representing the distribution of Pluto's near-infrared continuum absorbers, just as they failed to duplicate the spatial distribution of Pluto's ice species. This result is also consistent with recent visible maps of Pluto's sub-Charon hemisphere, which show a diversity of B-V colors in dark regions (Young *et al.* 2001). More complex models must be employed if we want to learn more about the distribution and

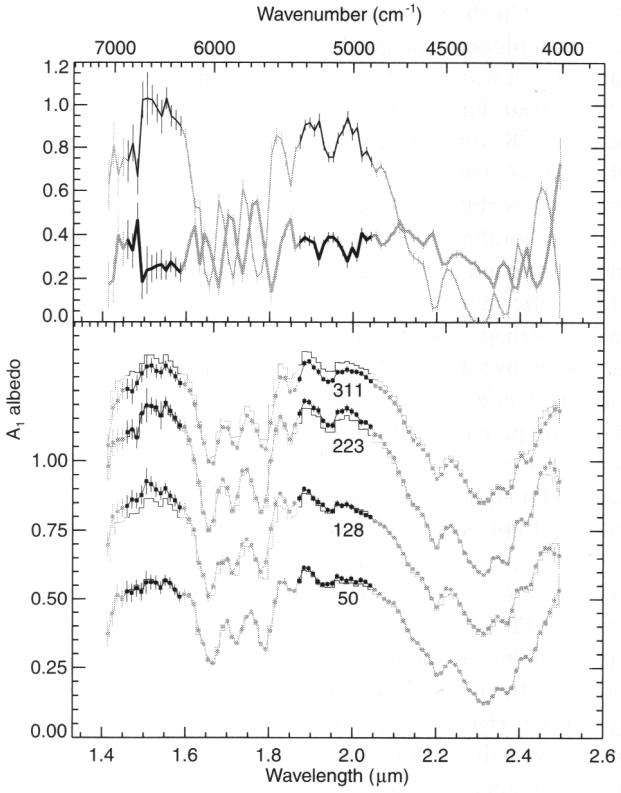

FIG. 6. Spectral end members derived from the assumption of a two-terrain Pluto surface are only of potential interest at continuum wavelengths (other wavelengths are shown in grey). The top panel shows the two end members; the bold curve represents the visually dark end member while the thin curve represents the bright end member. The bottom panel shows the fit of this model (stair-step curves) to the NICMOS data set (points). Reduced χ^2 of this fit is 7.

composition of the materials responsible for Pluto's continuum absorption.

3.2.2. *Three-Terrain Models*

We next investigated models having three distinct terrain types. With three-terrain models, a monochromatic albedo map cannot be used to uniquely constrain the placement of the terrains. Several different three-terrain maps have been proposed by Grundy and Fink (1996), Lellouch *et al.* (2000), and Grundy and Buie (2001), each accompanied by descriptions of the three terrains usable for computing Hapke multiple-scattering spectral models (Hapke 1993). These map/model combinations were devised to match the longitudinal variability of Pluto's CH_4 and N_2 absorption bands and/or Pluto's thermal infrared emission. Not having been implemented to fit continuum spectral regions, it is not surprising that they fail to match the longitudinal behavior of these spectral regions. For example, the Grundy and Buie (2001) modified HST map and model lead to a reduced χ^2 of 80 compared with the NICMOS data set.

By using the continuum information in the NICMOS data set to constrain a three-terrain model, one can obtain much better fits to the NICMOS data. Additional information is needed for at least one other aspect of the problem, either the spatial distribution of the three terrains, or their spectral properties. For this investigation, we tried both approaches to the task of fitting three-terrain models of Pluto's surface. First, we used previously proposed three-terrain maps (summarized by Grundy and Buie 2001), and solved for the three regional spectra to minimize χ^2 for the NICMOS data set. Second, we ignored the maps and solved for fractional coverages for each HST view, working from Hapke model terrain spectra like those proposed by Grundy and Fink (1996) and by Grundy and Buie (2001) for the three regions. An advantage of the first procedure is that, except to the extent that they influenced the proposed maps, human prejudices about the spectral and compositional characteristics of Pluto's terrains do not influence the end member spectra derived from the HST data set; the spectra are obtained via solution of a simple linear algebra problem. The second approach benefits from using real radiative transfer models based on plausible surface compositions, while not imposing any *a priori* spatial distributions on the three terrains. This approach is useful because Pluto's near-infrared continuum absorbers may not be spatially correlated with specific ice species, such as CH_4, N_2, and CO, whose longitudinal spatial distributions have been studied (e.g., Grundy and Buie 2001). Near-infrared continuum absorbers could likewise be unrelated to the visible wavelength continuum absorbers having spatial distributions known from the mutual event photometry and HST imaging upon which the earlier maps were based (e.g., Buie *et al.* 1997b, Stern *et al.* 1997, Young *et al.* 1999, 2001).

Method 1. Using the first method, a fit based on the modified Grundy and Fink map (Grundy and Buie 2001) reprojected to HST viewing geometry is shown in Fig. 7. This fit was accomplished by solving independently at each wavelength for the albedos of the three terrains in the map, minimizing residuals relative to disk-integrated albedos observed during all four HST/NICMOS observations. Overall χ^2 of the fit is 560, with reduced $\chi^2 = 5.9$. Similar quality of fit and similar spectra were obtained when we tried the modified HST map of Grundy and Buie (2001). The results do not appear to be especially sensitive to the differences between these maps, though limitations of the maps presumably do lead to impure derived end members.

Several things are interesting about the derived end member spectra. The spectrum obtained for the region specified in the maps as being bright and N_2-rich with dissolved CH_4 (dotted curve, right axis) does indeed exhibit high continuum albedos as well as CH_4 absorption bands shifted toward shorter wavelengths, consistent with CH_4 molecules isolated in β N_2 ice (e.g., Quirico and Schmitt 1997a). The spectrum derived for the CH_4-rich terrain (bold curve, right axis) shows stronger CH_4 absorption bands, with the longer wavelengths characteristic of CH_4 ice I. The spectral behaviors of these two terrains are entirely consistent with expectations from earlier work (e.g., Grundy and Fink 1996, Grundy and Buie 2001), although they are derived in an entirely new way, from an independent data set.

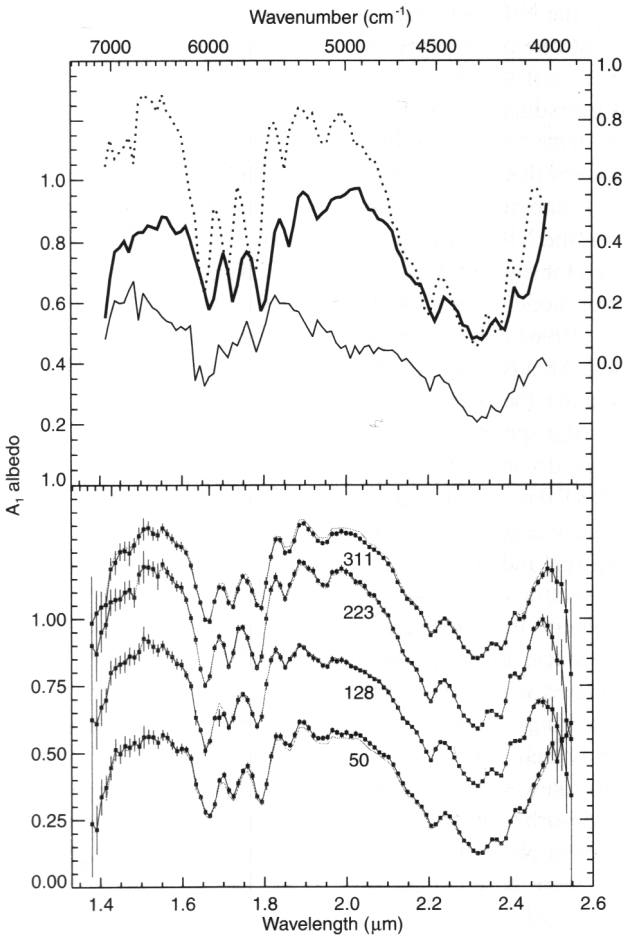

FIG. 7. Spectral end members derived for the modified Grundy and Fink map (Grundy and Buie 2001). The top panel shows the three end members; the dotted curve (right axis) is for the N_2-rich terrain, the bold curve (right axis) is for the CH_4-rich terrain, and the thin curve (left axis) is for the visually dark terrain. The bottom panel shows the fit of this model (gray curves) to the NICMOS data set (points). Reduced χ^2 of this fit is 5.9.

The NICMOS data are of particular interest for studies of continuum wavelengths difficult to observe from Earth, such as near 1.5 and 2.0 μm. Note the different continuum behaviors of the derived N_2-rich and CH_4-rich spectra, with the CH_4-rich spectrum showing much stronger and redder continuum absorption. This pattern is consistent with evolved organic residues accumulating in CH_4-rich regions, possibly because CH_4 ice is less volatile than N_2 so surfaces composed predominantly of it may tend to be older than N_2-rich terrains.

The third spectrum (thin, solid curve, left axis) is especially interesting. This spectrum corresponds to regions of the surface map which are dark at visible wavelengths. Its moderately high near-infrared albedos imply substantial redness, or increasing albedo with wavelength, between visible and near-infrared wavelengths, as reported by Grundy and Fink (1996). At near-infrared continuum wavelengths, the albedo is seen to decline toward longer wavelengths; what was reddish at shorter wavelengths is bluish in the near infrared. Albedos of this terrain are overall higher than albedos in the CH_4-rich regions at most near-infrared wavelengths. The higher near-infrared reflectivity of this terrain has the effect of elevating disk-integrated albedos near 128° longitude, changing Pluto's infrared continuum lightcurve as noted in Section 3.1. Some CH_4 absorptions are apparent, possibly resulting from the presence of CH_4 ice in this terrain and/or the effects of inaccuracies in the assumed map of Pluto mentioned earlier. Finally, at 1.55 and 2 μm, the continuum is noticeably depressed relative to typical CH_4-dominated spectra, perhaps pointing to the presence of H_2O ice in these regions, as hypothesized earlier (e.g., Grundy and Fink 1996, Cruikshank *et al.* 1997, Grundy and Buie 2001). This spectrum can be compared with the H_2O ice-dominated Charon spectrum shown in Fig. 1 to verify their similarity, particularly around 2 μm. Although it has long been anticipated on the surface of Pluto, and has been spectroscopically detected on the surface of Triton (e.g., Cruikshank *et al.* 1984, Hilbert *et al.* 1999, Cruikshank *et al.* 2000), H_2O has yet to be unambiguously detected on Pluto's surface. Considering the many assumptions implicit in this modeling procedure, we cannot claim a firm detection via the methods used here, but these results certainly do suggest that H_2O ice is present, and that it tends to outcrop in the most visually dark regions of Pluto's surface. However, it is far less obvious than the H_2O ice signature in spectra of Triton (e.g., Cruikshank *et al.* 2000), implying that H_2O ice is much less prominent on Pluto's surface than it is on Triton's.

Method 2. Our second approach involved iteratively adjusting the parameters of Hapke models of the three terrains proposed by Grundy and Buie (2001), seeking a set of three model spectra able to match the NICMOS data set with an arbitrary map. Accordingly, for each new set of model spectra, we computed fractional surface coverages for each HST observation to minimize residuals relative to disk-integrated spectra observed during all four observations. The best fits we found gave overall $\chi^2 = 1150$, twice the χ^2 of the previous model, but because fewer parameters were constrained, reduced χ^2 was much better at 3.4. One of these fits is shown in Fig. 8 and the fractional coverages required to minimize χ^2 for this model are compared with the fractional coverages in the previous map in Table II.

The derived coverage fractions are strongly dependent on details of the Hapke model spectra of the three terrains, and there is nothing particularly unique about the model spectra used here, so specific numbers in this table should not be given too much credence. However, the table does confirm that the N_2-rich terrain contributes most to the 223° observation while the CH_4-rich terrain was more widespread during the 50° and 311° observations. The visually dark terrain (composed of H_2O, carbon, and tholin, in this particular model) was prominent during the 128° observation. This distribution seems to hold, regardless of the model details. Scattering parameters for all three terrains shown in the top panel of Fig. 8 were taken from Grundy and Buie (2001). Detailed compositional parameters for the model shown in Fig. 8 are as follows.

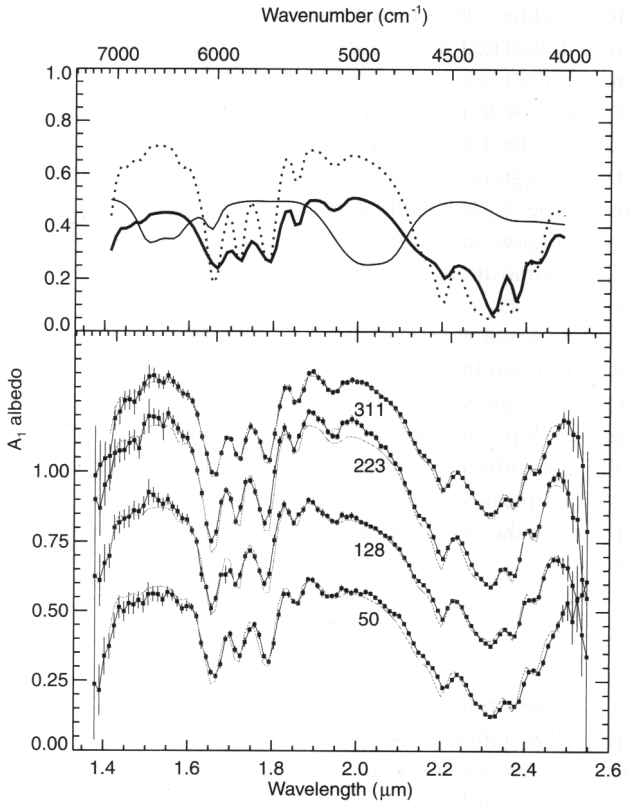

FIG. 8. Spectral end members based on Hapke models of three terrains similar to those proposed by Grundy and Buie (2001). The top panel shows the three end members; the dotted curve is N_2-rich, the bold curve is CH_4-rich, and the thin curve is rich in H_2O and tholin. The bottom panel shows the fit of this model (gray curves) to the NICMOS data set (points). Reduced χ^2 of this fit is 3.4.

- N_2-rich terrain: An intimate mixture of 20-cm and 1-cm grains, in the proportion 88 : 1 by volume, composed of β N_2 (Grundy *et al.* 1993) with 0.53% CH_4 and 0.45% CO ices dissolved in it by volume. Optical constants of the dissolved CH_4 were taken from Quirico and Schmitt (1997b), except at continuum wavelengths, where data from Grundy *et al.* (2001) were used. For CO ice, data from Legay–Sommaire and Legay (1982) and Quirico and Schmitt (1997b) were augmented with approximations from Grundy and Buie (2001). To this mixture was added 2% by volume 6 mm CH_4 ice I (Grundy *et al.* 2001) grains having 0.8% Titan tholin (khare *et al.* 1984) dispersed in them.

- CH_4-rich terrain: An intimate mixture of 12-mm and 0.1-mm grains, in the proportion 150 : 1 by volume, composed of 40 K CH_4 ice I (Grundy *et al.* 2001) with 0.4% Triton tholin (Khare *et al.* 1994) and 0.6% Titan tholin (Khare *et al.* 1984) dispersed in it.

- H_2O/tholin terrain: An intimate mixture of 50 μm grains of 60 K H_2O ice I_h (Grundy and Schmitt 1988) combined with 2.3% (by volume) 3-μm dark, carbon grains (Grundy and Buie 2001) and 0.5% 3-μm grains of Triton tholin (Khare *et al.* 1994).

It is important to stress that while these model terrains do locally minimize χ^2, they are unlikely to represent the best possible solution, and they say nothing about additional components which could be quite abundant without much influencing the near-infrared spectra. Many alternate configurations could produce similar or better fits. These ambiguities are inherent in the process of constructing complex spectral models (e.g.,Grundy 1995, Roush *et al.* 1996).

TABLE II
Fractional Coverages for Model Terrains

	Terrain type		
Sub-Earth longitude	N_2-rich	CH_4-rich	H_2O/tholin
	Fig. 7 model		
50	18%	43%	39%
128	37%	16%	46%
223	59%	25%	17%
311	29%	45%	26%
	Fig. 8 model		
50	61%	21%	17%
128	77%	0%	23%
223	89%	0%	11%
311	50%	44%	6%

4. DISCUSSION

In the previous section, our analyses of the HST/NICMOS data yielded several confirmatory results. First, the new data are consistent with earlier reports that the visually bright regions on Pluto are rich in N_2 and highly diluted CH_4 ice, and that these regions are highly reflective at near-infrared continuum wavelengths, just as they are at visual wavelengths. The data are also consistent with reports that regions rich in CH_4 ice I are more prevalent on the sub-Charon hemisphere (centered at 0° longitude), and that regions depleted in CH_4 and N_2 correspond to visually dark regions widespread near the minimum of Pluto's visual lightcurve (about 90° longitude).

Some intriguing new results have emerged from the analysis as well. The data point toward the existence of three distinct classes of continuum absorption on Pluto. To summarize, in bright, N_2-rich regions, there is little evidence for near-infrared continuum absorption by any species other than CH_4 ice. The weakness of continuum absorption by CH_4 (of order 0.1 to 0.001 cm^{-1}; Grundy *et al.* 2001) results in high continuum albedos and deep penetration of light at those wavelength (e.g., Grundy and Stansberry 2000). In CH_4-rich regions, we see a different pattern of continuum absorption, with a red slope extending through the near-infrared spectral range. Finally, a third pattern of continuum absorption with a steep red slope in the visible to ~1-μm range, but a neutral to blue continuum toward longer wavelengths seems to be associated with visually dark regions depleted in volatile ices. Because they are concentrated near 90°

longitude, these visually dark but infrared brighter regions make Pluto's near-infrared lightcurve differ at those longitudes from its visual lightcurve. Efforts to derive additional spectral characteristics of this enigmatic terrain hint at increased absorption around 2 μm, suggestive of the presence of H_2O ice.

Spectral identification of continuum absorbers is notoriously difficult; many species are capable of producing red or blue slopes similar to those exhibited by Pluto's terrains. Numerous silicate and organic species have reddish slopes in the visible and near infrared. Tholins have perhaps received the most attention, since they are expected to form via photochemical and radiolytic pathways (e.g., Strazzulla *et al.* 1984, Delitsky and Thompson 1987, Stren *et al.* 1988, Johnson 1989) both *in situ* within the ices on Pluto's surface as well as in Pluto's atmosphere, perhaps subsequently settling to the surface. Titan tholin, produced from simulated Titanian atmosphere (Khare *et al.* 1984), and also mixtures of Titan tholin and H_2O ice show patterns of absorption quite similar to what was derived for the dark, volatile-depleted terrain on Pluto, with a steep red slope from the visible to around $\sim$1 μm, then continuing level or with a blue slope toward longer wavelengths. A tholin formed under simulated Tritonian conditions (Khare *et al.* 1994) has a red slope continuing to longer near-infrared wavelengths, more like the pattern derived for Pluto's CH_4-rich terrain. The primary compositional difference between the Titan and Triton tholins is that the Titan tholin has a lower nitrogen content (McDonald *et al.* 1994). The continuum absorption profiles derived for Pluto's terrains suggest that tholins in Pluto's CH_4-rich terrains could be richer in nitrogen than tholins in volatile-depleted terrains.

Are the continuum characteristics derived for Pluto's terrains consistent with expectations from volatile transport models (e.g., Spencer *et al.* 1997, Trafton *et al.* 1997, 1998)? H_2O ice and tholins are nonvolatile at Pluto's surface temperatures, so regions where they are abundant are expected to be much older than surfaces composed of more mobile N_2, CO, and CH_4 ices. If dark, high molecular weight organic species settle out of the atmosphere and accumulate on Pluto's surface, they will progressively darken otherwise static surfaces. Darker patches absorb more sunlight, so they reach higher diurnal equilibrium temperatures; the heterogeneous distribution of these regions is indicated by Pluto's lightcurve in thermal emission (Lellouch *et al.* 2000). Solar heating drives sublimation of volatile ices and inhibits condensation from the atmosphere, leading to volatile depletion. However, during the winter, volatile species may perhaps be able to condense again in depleted regions, raising albedos, and starting the cycle anew. If Pluto's bulk atmospheric composition changes over the seasonal cycle, the composition of the tholins produced in the atmosphere could change as well. It may be that near aphelion, more nitrogen-rich tholins are formed because CH_4 is almost entirely absent from the thin residual atmosphere, while near perihelion, more carbon-rich tholins are formed. Tholins formed within Pluto's surface ices should reflect the compositions of the ices available in different regions. In CH_4-rich ice, one might expect carbon-rich tholins to form, while nitrogen-rich tholins would be expected to form in ices dominated by N_2 ice. However, the shapes of the continuum slopes derived from the NICMOS data suggest a different trend, with nitrogen-rich tholins accompanying CH_4-rich ice and carbon-rich tholins in volatile-depleted regions. Perhaps CH_4-rich regions are themselves lag deposits remaining after most of the N_2 has sublimated away from an older, darkened N_2-rich region, and tholins present in these regions reflect the earlier composition. Likewise, if the volatile-depleted regions were once CH_4-rich regions, their carbon-rich tholins could be providing fossil evidence of that history. However, it is important to bear in mind that compositions cannot be reliably derived from continuum slopes alone. Other species could influence the observed slopes as well. For example, H_2O ice depresses albedos in the near infrared, particularly near 2 μm. Perhaps H_2O absorption truncates the longer wavelength portion of an otherwise red slope in the volatile-depleted terrain, but not in the CH_4-rich terrain.

5. SUMMARY

We present four new near-infrared spectra of Pluto, obtained during 1998 with HST/NICMOS. The new data are used to study continuum absorption among Pluto's terrains, something which is particularly difficult to do by means of ground-based observations. We interpret the data using two-terrain and three-terrain compositional models of Pluto's surface. As was found with studies of Pluto's molecular absorption bands, two-terrain models are unable to match the rotational variations observed in Pluto's continuum spectrum. Three-terrain models give more reasonable results, and independently confirm earlier conclusions about the spatial distributions of CH_4 and N_2 ices on Pluto. The new data point to distinct continuum absorption patterns in each of the three terrains. In N_2-rich regions, there is very little continuum absorption, at both visible and near-infrared wavelengths. In CH_4-rich regions, a reddish near-infrared continuum slope is seen, consistent with N_2-rich Triton tholin. In volatile-depleted regions, the reddish slope observed from the visible to $\sim$1 μm gives way to a slightly blue slope in the near-infrared, suggestive of the presence of H_2O ice and/or something like carbon-rich Titan tholin. This latter terrain is dark at visible wavelengths, but is not especially dark in the near-infrared, so Pluto's lightcurve in the near-infrared is quite distinct from what is seen in the visible. Absorption features of H_2O ice are much less apparent in Pluto's spectrum than they are in Triton's spectrum.

ACKNOWLEDGMENTS

Special thanks to Alex Storrs for his valuable contribution to the successful execution of the Space Telescope observations. Thanks also to two anonymous reviewers for their helpful suggestions. Support for this work was provided by Grant HST-GO-07818.01-A by the Space Telescope Science Institute (STScI), which is operated by the Association of Universities for Research in

Astronomy, Inc., for NASA under Contract NAS 5-26555. Additional support for W. M. Grundy was provided by Hubble Fellowship Grant HF-01091.01-97A awarded by STScI, and by NASA Grant NAG5-10159 to Lowell Observatory.

REFERENCES

Benchkoura, A. I. 1996. Modelisation du transport de volatils à la surface des planètes et satellites glacés du systeme solaire: Application à Triton et Pluton. Ph.D. thesis, University Joseph Fourier, Grenoble.

Bohn, R. B., S. A. Sandford, L. J. Allamandola, and D. P. Cruikshank 1994. Infrared spectroscopy of Triton and Pluto ice analogs: The case for saturated hydrocarbons. *Icarus* **111**, 151–173.

Brown, M. E., and W. M. Calvin 2000. Evidence for crystalline water and ammonia ices on Pluto's satellite Charon. *Science* **287**, 107–109.

Buie, M. W., and U. Fink 1987. Methane absorption variations in the spectrum of Pluto. *Icarus* **70**, 483–498.

Buie, M. W., and W. M. Grundy 2000a. The distribution and physical state of H_2O on Charon. *Icarus* **148**, 324–339.

Buie, M. W., and W. M. Grundy 2000b. Continued evolution in the lightcurve of Pluto. *Bull. Amer. Astron. Soc.* **32**, 1083 (abstract).

Buie, M. W., D. J. Tholen, and L. H. Wasserman 1997a. Separate lightcurves of Pluto and Charon. *Icarus* **125**, 233–244.

Buie, M. W., E. F. Young, and R. P. Binzel 1997b. Surface appearance of Pluto and Charon. In *Pluto and Charon* (S. A. Stern and D. J. Tholin, Eds.), pp. 269–293. Univ. of Arizona Press, Tucson.

Buie, M. W., W. M. Grundy, and S. D. Kern 1999. Separate spectra of Pluto and Charon from HST/NICMOS. *Bull. Amer. Astron. Soc.* **31**, 1109.

Cruikshank, D. P., R. H. Brown, and R. N. Clark 1984. Nitrogen on Triton. *Icarus* **58**, 293–305.

Cruikshank, D. P., T. L. Roush, J. M. Moore, M. V. Sykes, T. C. Owen, M. J. Bartholomew, R. H. Brown, and K. A. Tryka 1997. The surfaces of Pluto and Charon. In *Pluto and Charon* (S. A. Stern and D. J. Tholin, Eds.), pp. 221–267. Univ. of Arizona Press, Tucson.

Cruikshank, D. P., B. Schmitt, T. L. Roush, T. C. Owen, E. Quirico, T. R. Geballe, C. de Bergh, M. J. Bartholomew, C. M. Dalle Ore, S. Douté, and R. Meier 2000. Water ice on Triton. *Icarus* **147**, 309–316.

Delitsky, M. L., and W. R. Thompson 1987. Chemical processes in Triton's atmosphere and surface. *Icarus* **70**, 354–365.

Douté, S., B. Schmitt, E. Quirico, T. C. Owen, D. P. Cruikshank, C. de Bergh, T. R. Geballe, and T. L. Roush 1999. Evidence for methane segregation at the surface of Pluto. *Icarus* **142**, 421–444.

Dumas, C., R. J. Terrile, R. H. Brown, G. Schneider, and B. A. Smith 2001. Hubble space telescope NICMOS spectroscopy of Charon's leading and trailing hemispheres. *Astron. J.* **121**, 1163–1170.

Grundy, W. M. 1995. Methane and Nitrogen Ices on Pluto and Triton: A Combined Laboratory and Telescope Investigation. Ph.D. thesis, University of Arizona, Tucson.

Grundy, W. M., and M. W. Buie 2001. Distribution and evolution of CH_4, N_2, and CO ices on Pluto's surface: 1995 to 1998. *Icarus* **153**, 248–263.

Grundy, W. M., and U. Fink 1996. Synoptic CCD spectrophotometry of Pluto over the past 15 years. *Icarus* **124**, 329–343.

Grundy, W. M., and B. Schmitt 1998. The temperature-dependent near-infrared absorption spectrum of hexagonal H_2O ice. *J. Geophys. Res.* **103**, 25809–25822.

Grundy, W. M., and J. A. Stansberry 2000. Solar gardening and the seasonal evolution of nitrogen ice on Triton and Pluto. *Icarus* **148**, 340–346.

Grundy, W. M., B. Schmitt, and E. Quirico 1993. The temperature dependent spectra of α and β nitrogen ice with application to Triton. *Icarus* **105**, 254–258.

Grundy, W. M., B. Schmitt, and E. Quirico 2001. The temperature dependent spectrum of methane ice I between 0.7 and 5 μm and opportunities for near-infrared remote thermometry. *Icarus* **155**, 486–496.

Hapke, B. 1993. *Theory of Reflectance and Emittance Spectroscopy*. Cambridge Univ. Press, New York.

Hilbert, B., J. A. Stansberry, W. M. Grundy, M. W. Buie, and R. V. Yelle 1999. The near-IR spectrum of Triton: Characterization and search for variability, presented at "Pluto & Triton," September 23–24, Flagstaff, AZ.

Johnson, R. E. 1989. Effect of irradiation on the surface of Pluto. *Geophys. Res. Lett.* **16**, 1233–1236.

Khare, B. N., C. Sagan, E. T. Arakawa, F. Suits, T. A. Callcott, and M. W. Williams 1984. Optical constants of organic tholins produced in a simulated Titanian atmosphere: From soft X-ray to microwave frequencies. *Icarus* **60**, 127–134.

Khare, B. N., C. Sagan, M. Heinrich, W. R. Thompson, E. T. Arakawa, P. S. Tuminello, and M. Clark 1994. Optical constants of Triton tholin: Preliminary results. *Bull. Am. Astron. Soc.* **26**, 1176–1177 (abstract).

Legay-Sommaire, N., and F. Legay 1982. Analysis of the infrared emission and absorption spectra from isotopic CO molecules in solid α-CO. *Chem. Phys.* **66**, 315–325.

Lellouch, E., R. Laureijs, B. Schmitt, E. Quirico, C. de Bergh, J. Crovisier, and A. Coustenis 2000. Pluto's non isothermal surface. *Icarus* **147**, 220–250.

Marcialis, R. L., and L. A. Lebofsky 1991. CVF spectrophotometry of Pluto: Correlation of composition with albedo. *Icarus* **89**, 255–263.

McDonald, G. D., W. R. Thompson, M. Heinrich, B. N. Khare, and C. Sagan 1994. Chemical investigation of Titan and Triton tholins. *Icarus* **108**, 137–145.

Owen, T. C., T. L. Roush, D. P. Cruikshank, J. L. Elliot, L. A. Young, C. de Bergh, B. Schmitt, T. R. Geballe, R. H. Brown, and M. J. Bartholomew 1993. Surface ices and atmospheric composition of Pluto. *Science* **261**, 745–748.

Quirico, E. 1995. Études spectroscopiques proche infrarouges de solides moleculaires: Application a l'etude des surfaces glacées de Triton et Pluton. Ph.D. thesis, University of Joseph Fourier, Grenoble.

Quirico, E., and B. Schmitt 1997a. Near-infrared spectroscopy of simple hydrocarbons and carbon oxides diluted in solid N_2 and as pure ices: Implications for Triton and Pluto. *Icarus* **127**, 354–378.

Quirico, E., and B. Schmitt 1997b. A spectroscopic study of CO diluted in N_2 ice: Applications for Triton and Pluto. *Icarus* **128**, 181–188.

Roush, T. L., D. P. Cruikshank, J. B. Pollack, E. F. Young, and M. J. Bartholomew 1996. Near-infrared spectral geometric albedos of Charon and Pluto: Constraints on Charon's surface composition. *Icarus* **119**, 214–218.

Schmitt, B., E. Quirico, F. Trotta, and W. M. Grundy 1998. Optical properties of ices from UV to infrared. In *Solar System Ices* (B. Schmitt, C. de Bergh, and M. Festou, Eds.), pp. 199–240. Kluwer Academic, Boston.

Spencer, J. R., J. A. Stansberry, L. M. Trafton, E. F. Young, R. P. Binzel, and S. K. Croft 1997. Volatile transport, seasonal cycles, and atmospheric dynamics on Pluto. In Pluto and Charon (S. A. Stern and D. J. Tholin, Eds.), pp. 435–473. Univ. of Arizona Press, Tucson.

Stansberry, J. A., and R. V. Yelle 1999. Emissivity and the fate of Pluto's atmosphere. *Icarus* **141**, 299–306.

Stansberry, J. A., J. R. Spencer, B. Schmitt, A. Benchkoura, R. V. Yelle, and J. I. Lunine 1996. A model for the overabundance of methane in the atmospheres of Pluto and Triton. *Planet. Space Sci.* **44**, 1051–1063.

Stern, S. A., L. M. Trafton, and G. R. Gladstone 1988. Why is Pluto bright? Implications of the albedo and lightcurve behavior of Pluto. *Icarus* **75**, 485–498.

Stern, S. A., M. W. Buie, and L. M. Trafton 1997. HST high-resolution images and maps of Pluto. *Astron. J.* **113**, 827–843.

Strazzulla, G., L. Calcagno, and G. Foti 1984. Build up of carbonaceous material by fast protons on Pluto and Triton. *Astron. Astrophys.* **140**, 441–444.

Trafton, L., D. M. Hunten, K. J. Zahnle, and R. L. McNutt 1997. Escape processes at Pluto and Charon. In *Pluto and Charon* (S. A. Stern and D. J. Tholin, Eds.), pp. 475–522. Univ. of Arizona Press, Tucson.

Trafton, L., D. L. Matson, and J. A. Stansberry 1998. Surface/atmosphere interaction and volatile transport (Triton, Pluto, Io). In *Solar System Ices* (B. Schmitt, C. de Bergh, and M. Festou, Eds.), pp. 773–812. Kluwer Academic, Boston.

Tryka, K. A., R. H. Brown, D. P. Cruikshank, T. C. Owen, T. R. Geballe, and C. de Bergh 1994. Temperature of nitrogen ice on Pluto and its implications for flux measurements. *Icarus* **112**, 513–527.

Young, E. F., K. Galdamez, M. W. Buie, R. P. Binzel, and D. J. Tholen 1999. Mapping the variegated surface of Pluto. *Astron. J.* **117**, 1063–1076.

Young, E. F., R. P. Binzel, and K. Crane 2001. A two-color map of Pluto's sub-Charon hemisphere. *Astron. J.* **121**, 552–561.